Nanoscale

PAPER

View Article Online
View Journal | View Issue

Cite this: *Nanoscale*, 2015, **7**, 12192

A novel approach for the synthesis of ultrathin silica-coated iron oxide nanocubes decorated with silver nanodots ($Fe_3O_4/SiO_2/Ag$) and their superior catalytic reduction of 4-nitroaniline†

Mohamed Abbas,[a,b] Sri Ramulu Torati[a] and CheolGi Kim*[a]

Received 25th April 2015,
Accepted 10th June 2015

DOI: 10.1039/c5nr02680f

www.rsc.org/nanoscale

A novel sonochemical approach was developed for the synthesis of different core/shell structures of $Fe_3O_4/SiO_2/Ag$ nanocubes and SiO_2/Ag nanospheres. The total reaction time of the three sonochemical steps for the synthesis of $Fe_3O_4/SiO_2/Ag$ nanocubes is shorter than that of the previously reported methods. A proposed reaction mechanism for the sonochemical functionalization of the silica and the silver on the surface of magnetic nanocubes was discussed in detail. Transmission electron microscopy revealed that the surface of Fe_3O_4/SiO_2 nanocubes was decorated with small Ag nanoparticles of approximately 10–20 nm in size, and the energy dispersive spectroscopy mapping analysis confirmed the morphology of the structure. Additionally, X-ray diffraction data were used to confirm the formation of both phases of a cubic inverse spinel structure for Fe_3O_4 and bcc structures for Ag in the core/shell structure of the $Fe_3O_4/SiO_2/Ag$ nanocubes. The as-synthesized $Fe_3O_4/SiO_2/Ag$ nanocubes showed a high efficiency in the catalytic reduction reaction of 4-nitroaniline to 4-phenylenediamine and a better performance than both Ag and SiO_2/Ag nanoparticles. The grafted silver catalyst was recycled and reused at least fifteen times without a significant loss of catalytic efficiency.

Introduction

Noble metal nanoparticles have been intensively studied because of their promising applications in various fields including biology and catalyst applications. Notably, silver (Ag) is considered an inexpensive material compared with other noble metals, such as gold (Au), platinum (Pt) and palladium (Pd), and also, Ag possesses good chemical and physical properties.[1] Furthermore, Ag nanoparticles (NPs) have extraordinary plasmon-resonant optical scattering properties that are used in optical applications such as signal enhancers, optical sensors, and biomarkers.[2–6] Additionally, Ag enhances the effect of radiation treatment in killing cancer cells.[2,7] Moreover, Ag NPs are recognized as a promising antimicrobial and disinfectant agent that can be used to treat infectious diseases[8–10] even for organisms that display antibiotic resistance.[11,12] In particular, the use of Ag NPs as a catalyst has drawn significant interest because Ag combines the characteristics of high reactivity and selectivity. Notably, catalyzing the reduction of 4-nitro organic compounds with Ag NPs has been accepted to be an alternative, effective and eco-friendly route to produce 4-amino organic compounds in industry.[13,14]

Iron oxide nanoparticles have also been comprehensively studied for biomedical applications such as in hyperthermia treatment for malignant cells, drug delivery, biosensors, magnetic resonance imaging contrast agents, magnetic separation and cell sorting, and these applications are due to the unique magnetic properties and biocompatibility of these nanoparticles.[15–22] Furthermore, iron oxide displays excellent activity in energy and catalyst applications,[23,24] and notably, magnetite (Fe_3O_4) is considered the most effective heterogeneous Fenton catalyst compared with other iron oxides,[25–28] because magnetite is the only oxide that displays Fe^{2+} in its structure, which enhances the production rate of $^{\bullet}OH$ radicals.[25,29]

In general, functional materials can be defined as any material that integrally combines two or more properties designed to meet specific requirements through tailored properties. Therefore, the combination of Ag nanoparticles and Fe_3O_4 nanocubes to form core/shell nanostructures will offer

[a]*Department of Emerging Materials Science, Daegu Gyeongbuk Institute of Science and Technology (DGIST), 711-873 Daegu, South Korea. E-mail: cgkim@dgist.ac.kr; Fax: +82-53-785-6509; Tel: +82-104435-6632*
[b]*Ceramics Department, National Research Centre, El-Bohous Street, 12622 Cairo, Egypt*
†Electronic supplementary information (ESI) available. See DOI: 10.1039/c5nr02680f

possibilities for the development of advanced composite materials and create a promising composite for multiple applications. This nanostructure combines excellent magnetic responses, plasmonic properties, surface to volume ratios, bioconjugation affinities and biocompatibilities. However, naked iron oxide NPs are likely to form an aggregation and be easily oxidized or dissolved in an acidic medium during the recycling process. Thus, a protective layer for the iron oxide is required, and the best candidate for this layer is silica because of its high chemical and thermal stabilities.

Currently, to the best of our knowledge, few studies have been reported on the synthesis of MNPs/SiO_2/Ag nanoparticles with a spherical shape. Du *et al.*, Chi *et al.* and Shin *et al.* have succeeded in depositing Ag on silica coated Fe_3O_4 microspheres using combination approaches of solvothermal and Stober sol–gel processes for the catalytic reduction of 4-nitrophenol.[1,30,31] Wang *et al.* have succeeded in synthesising Fe_3O_4/SiO_2/Ag microspheres for the usage of antibacterial materials against *Escherichia coli*.[32] Bayat *et al.* have demonstrated the synthesis of Fe_3O_4/SiO_2/Ag nanocomposites using chemical methods for the oxidant-free dehydrogenation of alcohols.[33] Kooti *et al.* have successfully synthesized the $CoFe_2O_4$/SiO_2/Ag composite through a three-step procedure for using it as an antibacterial agent of both Gram-positive and Gram-negative bacteria.[34] Even though the majority of the aforementioned developed approaches are efficient and eclectic, the procedures used for preparing that type of functionalized nanoparticles are rather complicated and time-consuming. Furthermore, most of the methods are used to produce materials of microparticle size, which obviously affect their performance in the applications compared with using the nanoscale sized particles. Moreover, in several methods the reaction conditions are rather critical and require a substantial amount of surfactant and protective conditions. These requirements involve significant costs, and restricts the materials towards the industrial applications.

In this study, we report a new and rapid approach based on ultrasonication at high temperatures and pressure for the synthesis of Fe_3O_4/SiO_2/Ag nanocubes using three simple steps for a sonochemical reaction within a short time. Moreover, using the same approach of ultrasound, we synthesized a stable colloidal solution of Ag NPs and Ag decorated SiO_2 (SiO_2/Ag) nanospheres. The physical properties generated from ultrasonication, the microjet and shock waves could be the key parameters for enhancing the surface functionalization of iron oxide nanocubes in both the silica shell and silver nanoparticles. The morphology and crystal structures were monitored using different analysis techniques such as X-ray diffraction (XRD), transmission electron microscopy (TEM), high resolution transmission electron microscopy (HRTEM), and energy-dispersive X-ray spectroscopy (EDS) mapping, and using a superconducting quantum interference device (SQUID) for measuring the magnetic properties. The application efficiency of our produced sample was investigated in terms of the catalytic reduction of 4-nitroaniline to 4-phenylenediamine and the recycling properties.

Experimental details

Materials

Iron(II)sulfate heptahydrate ($FeSO_4 \cdot 7H_2O$), tetraethyl orthosilicate (TEOS), silver nitrate ($AgNO_3$), polyvinylpyrrolidone (PVP; M.W. 40 000), 4-nitroaniline, polyethylene glycol (PEG), sodium hydroxide (NaOH), ammonia, and ethyl alcohol (C_2H_5OH) (99%) were purchased from Sigma-Aldrich, Ltd. All chemicals were of analytical reagent grade and were used as received without any further purification. The synthesis process was performed under ambient temperature.

Synthesis of iron oxide (Fe_3O_4) nanocubes using the sonochemical method

The synthesis of Fe_3O_4 nanocubes was performed based on our previous studies.[35,36] In brief, 2.31 g of $FeSO_4 \cdot 7H_2O$ was dissolved in 100 mL of distilled water, and the solution was then transferred to the ultrasonication reactor chamber. NaOH was then injected into the reaction mixture within 15 min of initiating the ultrasonication. The reaction was continued for 70 min, and the ultrasonication was then halted. The obtained iron oxide nanocube was washed several times with water and ethanol. The precipitate was collected using a magnet, and then dried in a vacuum evaporator. The ultrasonic equipment is an ultrasonic processor (VibraCell-VCF1500, Sonics and Materials) with a maximum power of 1500 W. The sonoreactor was equipped with a titanium horn with a 5 cm^2 irradiating surface area and a piezoelectric transducer supplied by a 20 kHz generator submerged below the surface of the sonicated liquid.

Synthesis of Fe_3O_4/SiO_2 nanocubes using an ultrasonic assisted sol–gel method

The synthesis of Fe_3O_4/SiO_2 nanocubes followed our developed sol–gel approach[36] with modifications mainly in the use of ultrasound to reduce the reaction time. Typically, two short reactions of 30 minutes each using the ultrasonic assisted sol–gel methods were used to coat the Fe_3O_4 nanocubes with an ultrathin SiO_2 shell. In the first step, we functionalized the surface of the Fe_3O_4 NCs with PVP as follows: 4 g of PVP was dispersed in 60 mL distilled H_2O and was then mixed with 100 mg Fe_3O_4 dispersed in 20 mL distilled H_2O under ultrasonication for 30 min. In the second step, we added the PVP-stabilized Fe_3O_4 to a solution containing 100 mL of ethyl alcohol and 5 mL ammonia and ultrasonicated for 30 min. During the ultrasonication, we injected 1.5 mL of TEOS into the solution. Thereafter, the solution was washed several times with ethanol and water. The precipitate of Fe_3O_4/SiO_2 nanocubes was collected using a magnet.

Synthesis of Fe_3O_4/SiO_2/Ag nanocubes using the sonochemical method

To functionalize the surface of Fe_3O_4/SiO_2 nanocubes with Ag, we used a one pot-sonochemical reaction. In a typical synthesis of Fe_3O_4/SiO_2/Ag nanocubes, 35 mg of the prepared Fe_3O_4/SiO_2 nanocubes were dispersed in a mixed solution of

100 mL ethanol and 5 mL ammonia. The samples were ultrasonicated for 10 min, and after the ultrasonication, a solution of 0.4 g $AgNO_3$ dispersed in 20 mL ethanol was rapidly injected and finally sonicated for another 30 minutes. To prepare a solution of $AgNO_3$ in ethanol, we employed ultrasonication because the silver nitrate cannot solubilize as easily in ethanol as in water. The reaction was halted, and the obtained mixture was washed several times with water and ethanol. The precipitate was collected using a magnet and then dried in a vacuum evaporator to obtain the core/shell nanocubes of $Fe_3O_4/SiO_2/Ag$.

Synthesis of silica (SiO_2) nanoparticles using the sonochemical method

For the synthesis of SiO_2 NPs, we used a one-pot reaction of the sonochemical method. Typically, 3 mL of TEOS was added to a 100 mL solution of dis. H_2O and ethanol and 5 mL of ammonia with stirring for 5 min. After that, the solution was transferred to the ultrasonication reactor chamber. The reaction was continued for 50 min, and the ultrasonication was then turned off. The obtained SiO_2 NPs were washed several times with water and ethanol, and the precipitate was collected by centrifusion, and then dried in an oven at 90 °C for 6 h.

Synthesis of silver decorated silica (SiO_2/Ag) nanoparticles using the sonochemical method

The synthesis of Ag decorated SiO_2 nanoparticles is shown in Scheme 1b. For the functionalization of the surface of SiO_2 with Ag nanodots, we used the same sonochemical procedures with slight modification. Typically, 100 mg of the prepared SiO_2 NPs were dispersed in a mixed solution of 100 mL ethanol and 5 mL ammonia for 5 min using a magnetic stirrer. The solution was then transferred to the ultrasonication reactor chamber. After 10 min of ultrasonication, a solution of $AgNO_3$ dispersed in ethanol was rapidly injected and the reaction was continued for 40 min. The reaction was halted, and the obtained SiO_2/Ag core/shell was washed several times with water and ethanol. The precipitate was collected using centrifusion, and then dried in an oven at 90 °C for 6 h.

Synthesis of silver (Ag) nanoparticles using the sonochemical method

The synthesis of yellow stable colloidal Ag NPs was performed using an eco-friendly rapid sonochemical method. Typically, 0.2 g of $AgNO_3$ was dispersed in a mixed solution of 1 : 1 dis. H_2O : ethanol using a magnetic stirrer for 5 min. After that, 10 mL of PEG was added and then the solution was transferred

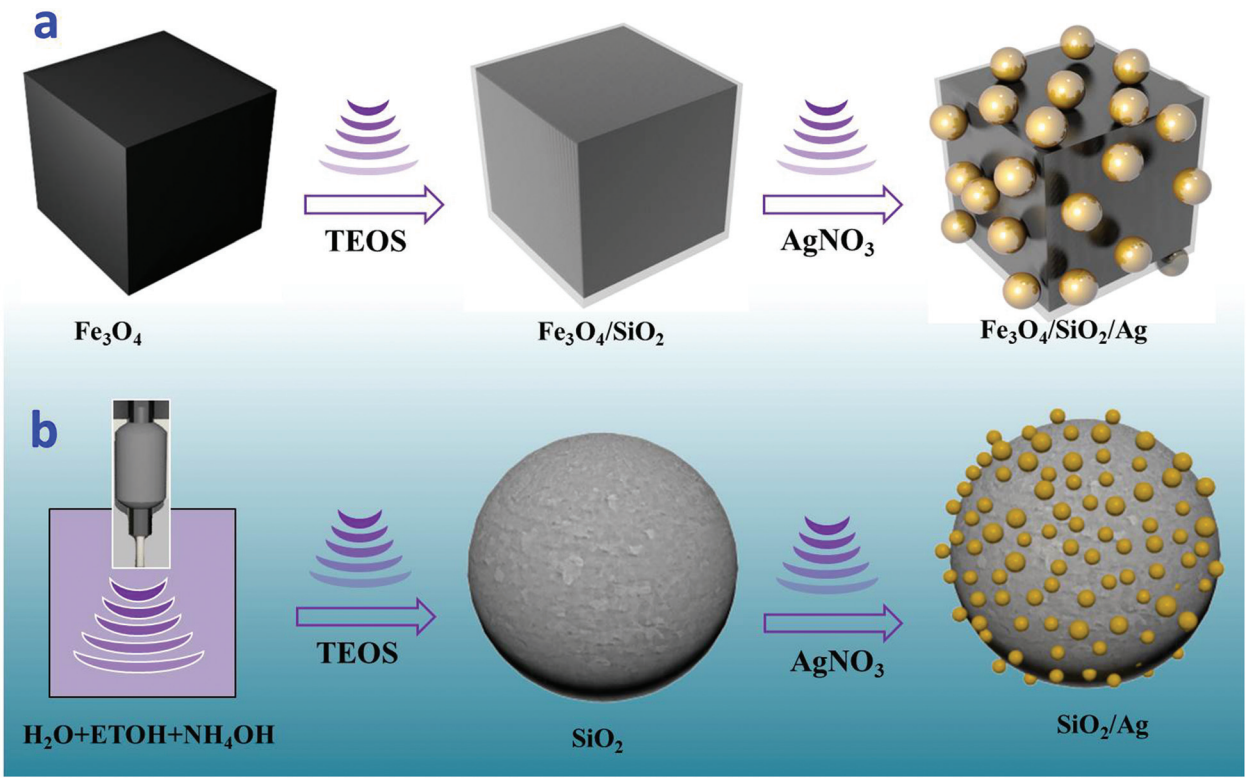

Scheme 1 Schematic diagram illustrating the synthesis process of (a) the silver-decorated silica-coated iron oxide ($Fe_3O_4/SiO_2/Ag$) nanocubes and (b) the silver-decorated silica (SiO_2/Ag).

to the ultrasonication reactor chamber. The reaction was continued for 30 min and then turned off. The obtained Ag colloidal NPs with yellow color were washed several times with water and ethanol, and the precipitate was collected using centrifusion.

Catalytic test

To study the efficiency of our synthesized $Fe_3O_4/SiO_2/Ag$ nanocube sample as a catalyst material, we used the nanocubes in the catalytic reduction reaction of 4-nitroaniline to 4-phenylenediamine. In a typical catalysis reaction, 100 μL of 1 mM 4-nitroaniline, 100 μL of 10 mM $NaBH_4$ and 100 μL of 1 mM of $Fe_3O_4/SiO_2/Ag$ nanocubes were mixed with 700 μL of ultrapure water. The chemical reduction of 4-nitroainilne was monitored using a UV-visible spectrophotometer in quartz cuvettes with a 1 cm path length and with freshly prepared solutions. The same procedures were used to study the catalytic activity of the other two catalyst materials of Ag and SiO_2/Ag nanoparticles. To study the recycling of the as-synthesized Ag-decorated silica-coated iron oxide nanocubes, the same procedure was repeated in up to 15 cycles. The functionalized nanocubes were separated from the mixture using a permanent magnet, washed three times with deionized water and then reused in the next cycle.

Analysis methods

The morphology of the functionalized core/shell nanocubes ($Fe_3O_4/SiO_2/Ag$), SiO_2/Ag and Ag NPs was observed by TEM (Tecnai G2 F20 operated at 300 kV), and the chemical compositions of the nanocubes were analyzed by an EDS mapping analysis coupled with the TEM equipment. X-ray diffraction (XRD) patterns were collected (Regaku D/max-2500) at a voltage of 40 kV, a current of 300 mA and a scanning rate of 2° min^{-1} with a step size of 0.01°. The catalytic reduction of 4-nitroaniline was characterized by a NANODROP 2000c spectrophotometer (Thermo Scientific) operated at a resolution of 1 nm using freshly prepared solutions in quartz cuvettes with a 1 cm path length. The magnetic properties of the functionalized core/shell nanocubes were measured by SQUID with an external magnetic field ranging from −15 kOe to +15 kOe.

Results and discussion

The synthesis approach for the silver-decorated silica-coated iron oxide nanocubes has been performed by three sonochemical routes. A schematic overview of the formation of the functionalized nanocubes is shown in Scheme 1a. The total reaction time for the synthesis of the core/shell nanostructure is shorter than that of the previously reported methods. The iron oxide nanocubes were synthesized by our sonochemical method as described previously.[35,36] The morphology of the as-synthesized iron oxide nanocubes is shown in Fig. 1. As revealed by TEM, Fig. 1(a, b) show that the obtained Fe_3O_4 nanocubes have a mean diameter of 40 nm and are approximately cubic-like in shape. In addition, we have performed scanning electron microscopy for the synthesized nanoparticles and the results are shown in Fig. S1.†

However, the surface coating of Fe_3O_4 nanocubes with an ultrathin silica layer was performed within one hour using an ultrasonic assisted sol–gel method. In our previous work, we developed a modified sol–gel method to coat Fe_3O_4 with silica; however, we required four hours to complete that reaction. Based on the unusual reaction condition generated from the ultrasound of high temperatures and pressures, we succeeded in decreasing that time to one hour. The shock waves, microjets and turbulent flows resulting from the collapse of microbubbles can cause the collision of nanoparticles at velocities of hundreds of meters per second. This process forms the silica sol as a consequence of the decomposition of TEOS after injection toward the magnetite surface at high speeds, forming Fe_3O_4/SiO_2 core–shell nanocubes.[37–39] As observed in Fig. 1(c, d), the ultrathin silica coated magnetite nanocubes exhibit a cubic-like structure with a smooth surface and represent core/shell nanostructures. The size of the ultrathin silica layer around the Fe_3O_4 nanocubes is approximately 1.56 nm. HRTEM was used to observe the detailed structure of the Fe_3O_4/SiO_2 core/shell nanocubes (Fig. 2). The images clearly show the single-crystallinity of the Fe_3O_4 core and the amorphous nature of the silica shell. The interplanar distance measured from the adjacent lattice fringes in Fig. 2a is about 0.48 nm, corresponding to the (111) planes of the Fe_3O_4 single crystal with cubic inverse spinel structure.[40]

The functionalization process of the Fe_3O_4/SiO_2 nanocubes with silver to obtain the $Fe_3O_4/SiO_2/Ag$ NC nanostructures is also performed in the one-pot sonochemistry reaction. In general, the ultrasonication of an aqueous medium will produce the radicals $H^{\bullet}$ and $OH^{\bullet}$; these radicals can either recombine to return to their original form or combine to produce H_2 and H_2O_2, and strong oxidants and reductants were used to enhance the reaction.[41] However, in an alcohol medium (as in our reaction) two different types of radicals ($CH_3^{\bullet}$ and $CH_2OH^{\bullet}$) are expected to be generated, thereby enhancing the reaction.[42] The generated radical in the alcohol medium is expected to reduce the injected $AgNO_3$ to form Ag^{+}. In the presence of ammonia, $Ag(NH_3)_2^{+}$ will form and then reduce to Ag nanoparticles as suggested by Pol *et al.*[39] The stable complex of Ag $(NH_3)_2^{+}$ can be electrostatically attracted to the partially negatively charged SiO_2 shell. After sonication, the Ag bonds on the silica (SiO_2) and the mechanism of silver bonding to the silica surface are related to the physical properties of ultrasound (the microjets and shock waves created after the collapse of the bubbles).[43] Fig. 3 shows the TEM images of the $Fe_3O_4/SiO_2/Ag$ nanocubes. From the figure, small well-dispersed silver seeds were noted to attach to the surface of the Fe_3O_4/SiO_2 nanocubes, while maintaining the shape and the size of the core/shell Fe_3O_4/SiO_2 NCs. The developed sonochemical approach in our study is economical by providing a time-reducing, clean, eco-friendly and efficient route for the synthesis of $Fe_3O_4/SiO_2/Ag$ nanocubes at room temperature conditions without the need for high temperatures, surfactants or toxic chemicals. Thus, sonochemical pro-

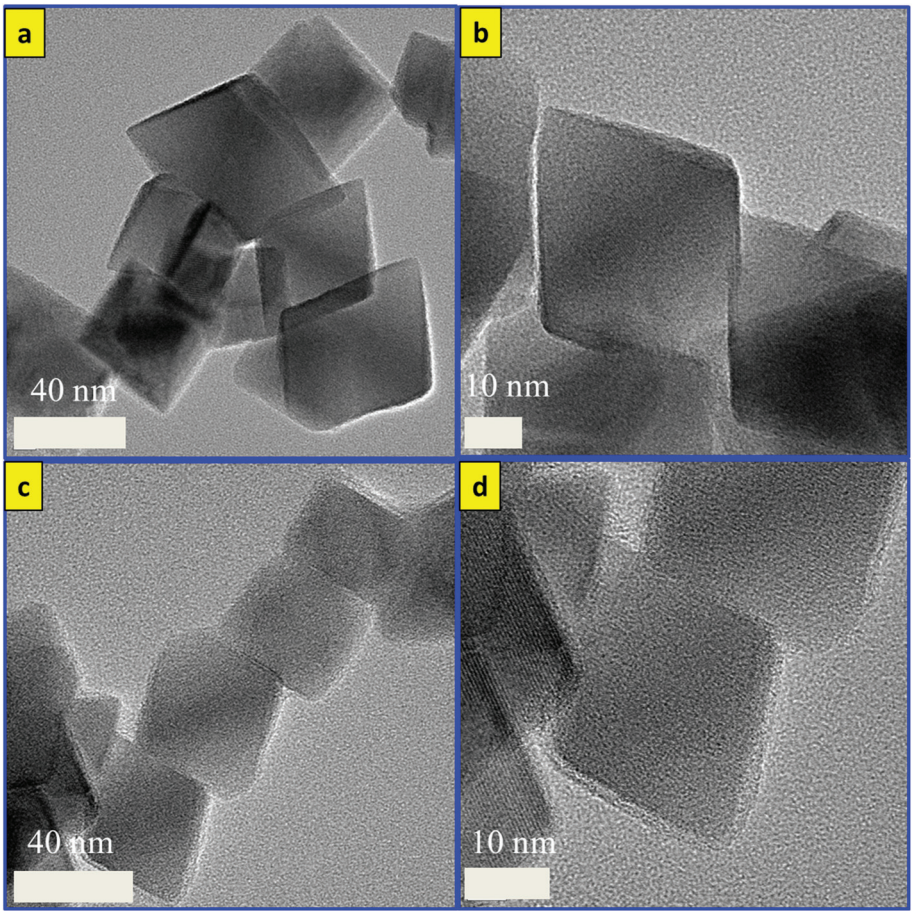

Fig. 1 TEM images of (a, b) as-prepared Fe_3O_4 nanocubes and (c, d) Fe_3O_4/SiO_2 nanocubes.

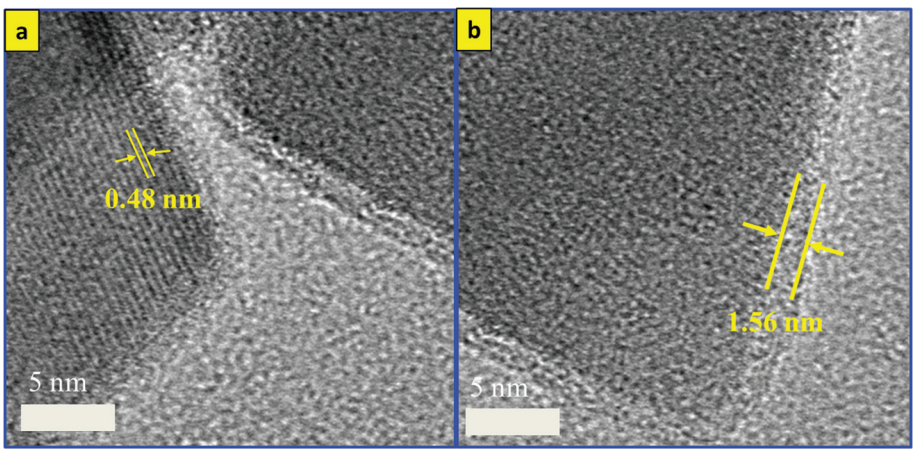

Fig. 2 HRTEM images of Fe_3O_4/SiO_2 nanocubes.

cessing for the production of functionalized nanocubes could be attractive for industrial applications.

The phases and purity of the synthesized samples were investigated using XRD. Fig. 3c shows the XRD patterns of three samples of Fe_3O_4, Fe_3O_4/SiO_2, and Fe_3O_4/SiO_2/Ag nanocubes. From the figure, all of the diffraction peaks of the crystal planes (220), (311), (400), (422), (511), and (440) could be indexed to a cubic inverse spinel for Fe_3O_4 NCs (JCPDS card number: 00-019-0629). The XRD pattern of Fe_3O_4/SiO_2 nanocubes exhibited identical features to pristine Fe_3O_4. However,

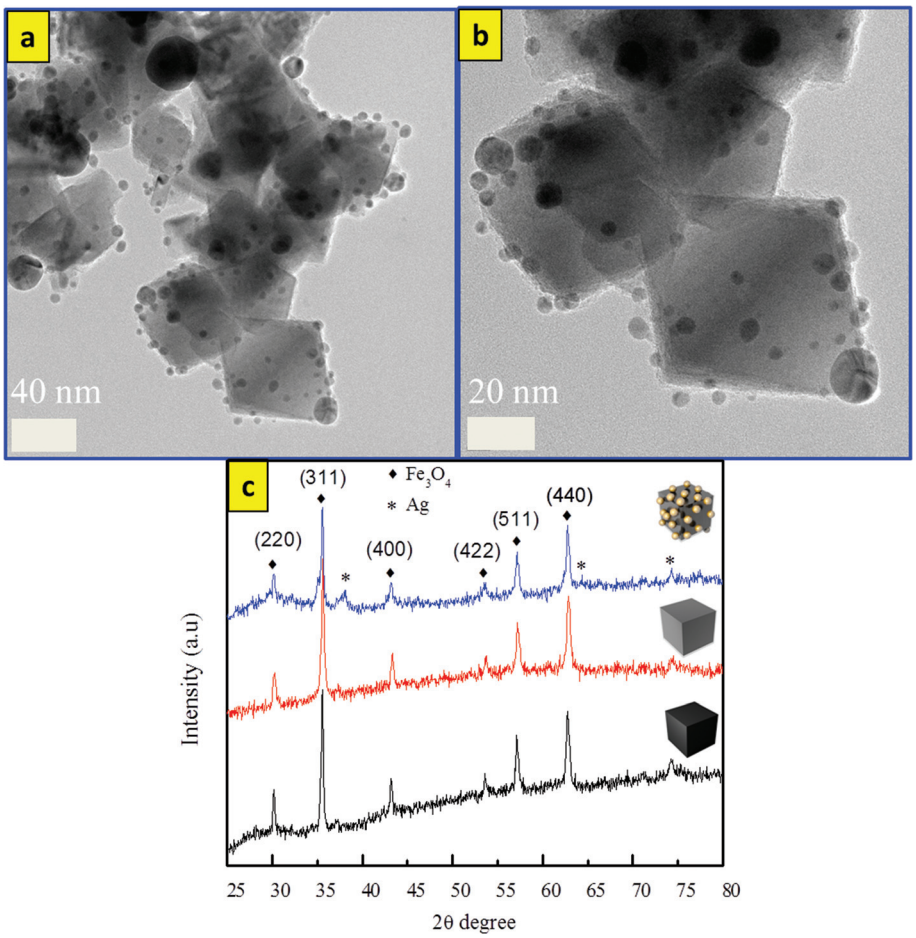

Fig. 3 TEM images of (a, b) $Fe_3O_4/SiO_2/Ag$ nanocubes and (c) the XRD pattern of Fe_3O_4, Fe_3O_4/SiO_2, and $Fe_3O_4/SiO_2/Ag$ nanocubes.

additional peaks at 2θ = 38° and 64.3° were observed for the core/shell structures of $Fe_3O_4/SiO_2/Ag$ nanocubes, which can be indexed to the face-centered cubic structure of Ag,[31] confirming the presence of the two phases in the core/shell nanocubes. The crystallite sizes of the three samples of Fe_3O_4, Fe_3O_4/SiO_2, and $Fe_3O_4/SiO_2/Ag$ nanocubes were calculated from the XRD pattern using the Debye–Scherrer formula ($D = K\lambda/\beta\cos\theta$), where λ is the X-ray wavelength (1.540562 Å), β is the full width at half maximum (FWHM), θ is the Bragg angle for the studied peak/ring, and K is the shape factor, which is normally taken as 0.9 for ferrites.[44] The crystallite sizes were calculated to be 30, 32, and 35 nm, which are smaller compared to the particle sizes estimated by TEM images as mentioned above. The reason for such a difference in size may be ascribed to the inhomogeneous strain and instrumental effects,[45] which may contribute to the width of the diffraction peak apart from the crystallites, resulting in smaller value for the estimations using the Scherrer equation.[46] Fig. 4 shows the EDS mapping images of $Fe_3O_4/SiO_2/Ag$ core/shell nanocubes indicating the spatial distribution of iron, oxygen, silicon and silver. Fig. 4(a) shows the TEM image of the silver-decorated silica-coated iron oxide nanocubes which are to be analyzed in the EDS mapping. Fig. 4(b) displays the elemental maps of all of the elements together, and Fig. 4(c–f) display the elemental maps of Fe, O, Si, and Ag individually. The elemental mapping results show that all elements were well distributed.

The magnetic hysteresis loops for the prepared Fe_3O_4, Fe_3O_4/SiO_2, and $Fe_3O_4/SiO_2/Ag$ nanocubes were measured using SQUID at room temperature (Fig. 5). The saturation magnetization value for the bare magnetite nanocubes at 300 K is 79.5 emu g^{-1}, and this value decreased for the samples coated with silica to 62.2 emu g^{-1}. The deposition of silver on Fe_3O_4/SiO_2 nanocubes causes a further decrease in the saturation magnetization value to 25.5 emu g^{-1}. A portion of this decrease in the magnetization value is because of the mass effect of silica and silver, and the remaining portion is because of diamagnetic shielding.[30] The further decrement in the magnetization value after silver deposition is also ascribed to the slight increase in the mass and size of the composite. The coercivity as well as remanent magnetization values of Fe_3O_4 NCs were also affected by the coating process. The Hc and Mr values of Fe_3O_4 were changed from 100 Oe and 7 emu g^{-1} to 145 Oe and 4 emu g^{-1} for the functionalized sample of $Fe_3O_4/SiO_2/Ag$ NCs. These changes in the values may be understood in terms of the change in the domain structure or surface anisotropy upon coating.[34] The bifunctional nano-

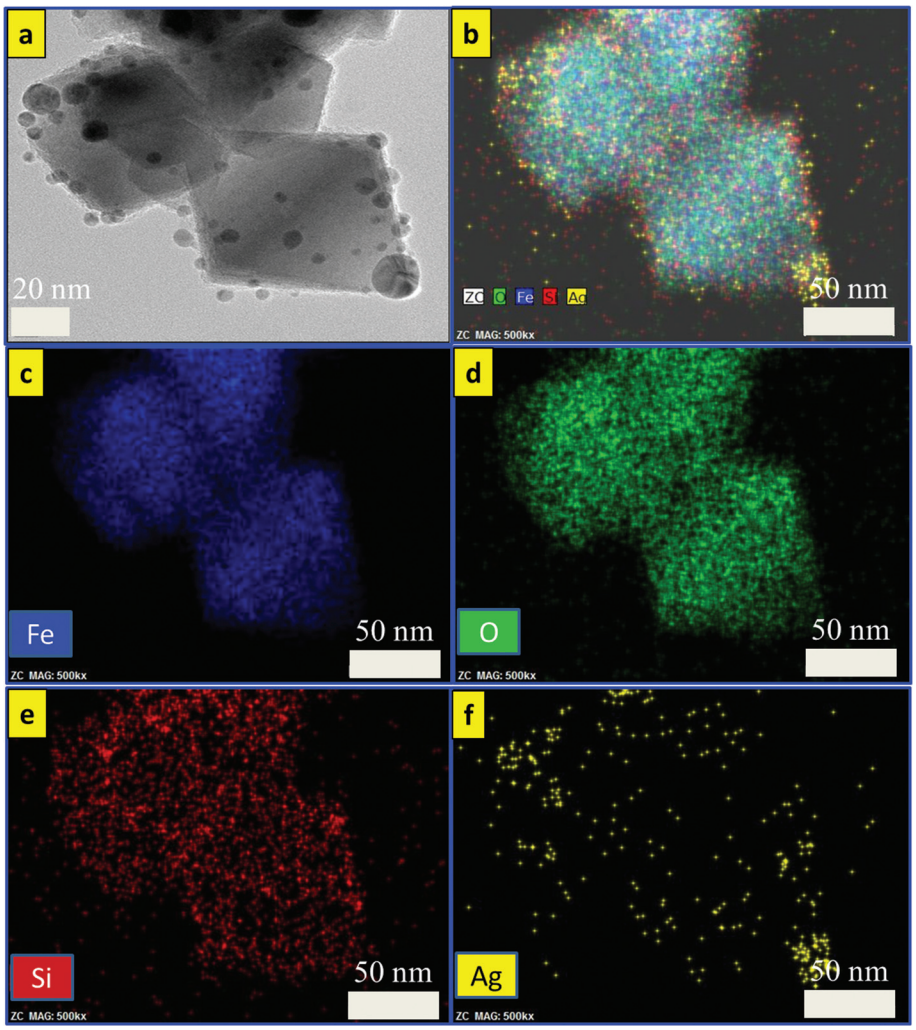

Fig. 4 EDS mapping analysis of $Fe_3O_4/SiO_2/Ag$ nanocubes.

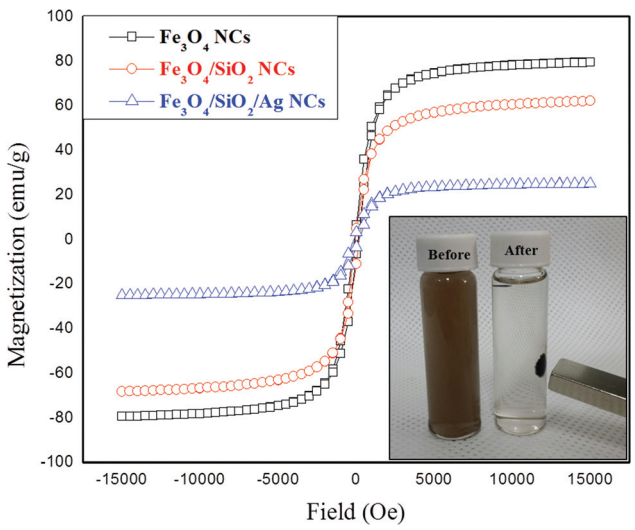

Fig. 5 The magnetization curves for Fe_3O_4, Fe_3O_4/SiO_2 and $Fe_3O_4/SiO_2/Ag$ nanocubes measured by SQUID at 300 K and a photograph of $Fe_3O_4/SiO_2/Ag$ nanocubes in water in the absence and presence of an external magnet (inset).

composites still displayed a strong magnetization, suggesting their suitability for magnetic separation and targeting.[47] Therefore, these particles can be rapidly separated from solution using an external magnetic field (inset of Fig. 5), achieving reusability.

On the other hand, Ag, SiO_2, and silver decorated silica (SiO_2/Ag) nanoparticles were synthesized for the comparison of catalytic properties with $Fe_3O_4/SiO_2/Ag$ nanocubes using the same developed sonochemical approach in a short time. At first, SiO_2 nanoparticles with a size distribution range of 100 nm were synthesized in rapid sonochemical reaction within 30 min. Fig. 6(a, b) show TEM images of SiO_2 NPs and the particles have spherical morphology. The functionalization of the SiO_2 surface with Ag nanodots was performed in a one-pot sonochemical reaction. The mechanism for obtaining such Ag decorated SiO_2 nanoparticles is mainly attributed to the physical properties of ultrasound and the electrostatic attraction between the different charges of SiO_2 and Ag. Fig. 6(c, d) show the TEM images of the silver decorated silica

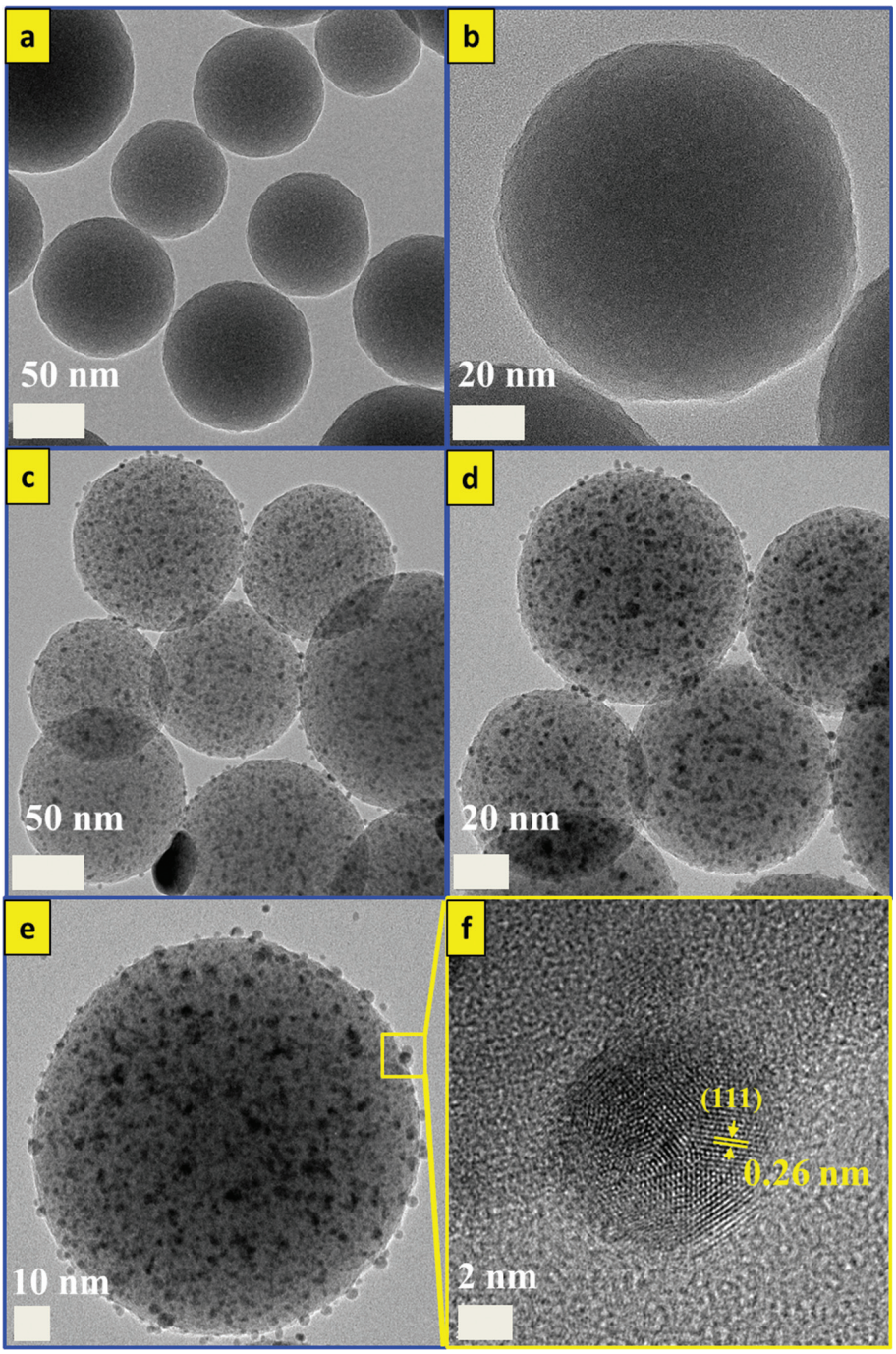

Fig. 6 TEM images of (a, b) SiO_2 NPs, (c, d) SiO_2/Ag NPs, and (e, f) HRTEM of SiO_2/Ag NPs.

nanoparticles with different resolutions. Fig. 6(e, f) show HRTEM images of SiO_2/Ag NPs, and the lattice spacing calculated from the figure is found to be almost 0.26 nm and corresponds to the (111) lattice plane of the face centered cubic (FCC) structure of silver.[48,49] Fig. 7 shows the EDS mapping images of Ag decorated SiO_2 nanoparticles indicating the spatial distribution of silicon, silver and oxygen. Fig. 7(b) displays the elemental maps of all of the elements together in Ag decorated SiO_2 nanoparticles, and Fig. 7(c–e) display the elemental maps of Si, Ag and O separately. The well distributions of the elements are observed in elemental mapping images. For the synthesis of colloidal Ag nanoparticles, we used an eco-friendly one-pot sonochemical reaction, in which the PEG was used as a reducing agent as well as a stabilizing agent. Fig. 8a and b show TEM images for well dispersed Ag nanoparticles with different resolutions. The Ag nanoparticles

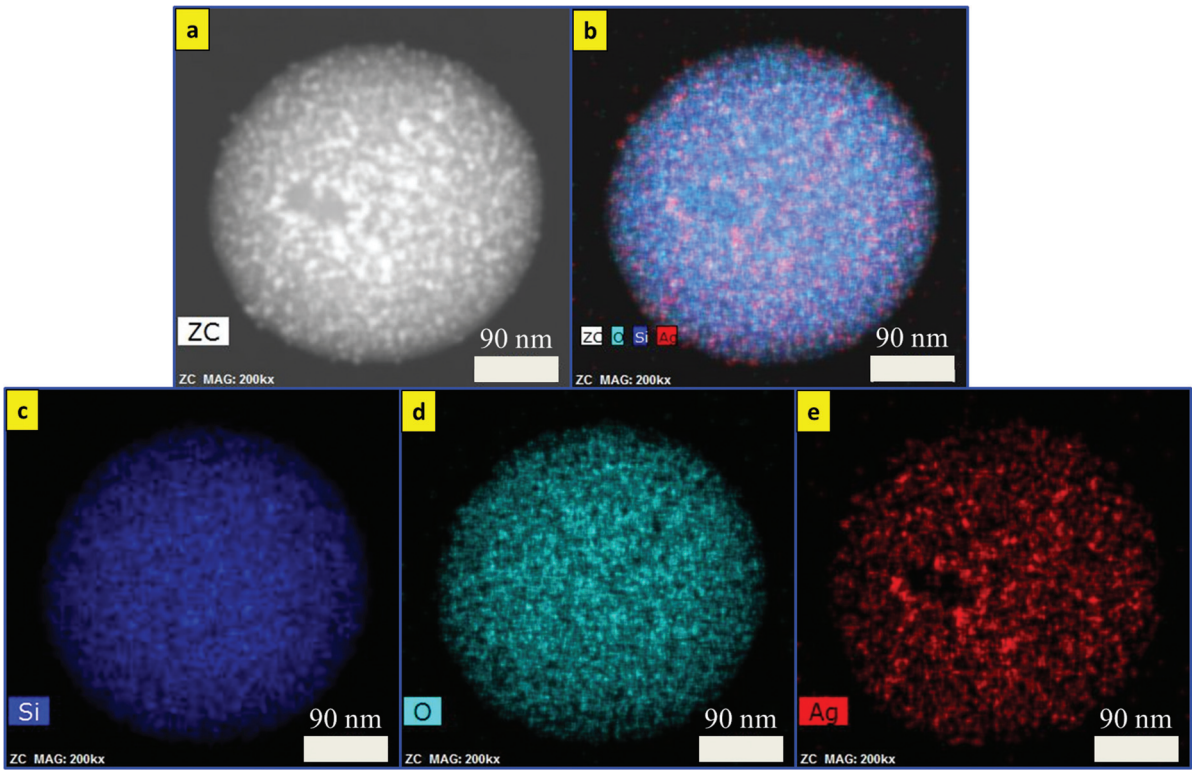

Fig. 7 EDS mapping analysis of SiO_2/Ag nanoparticles.

have an average size distribution of 15 nm with a spherical shape. Fig. 8c shows the HRTEM image of Ag nanoparticles and the interplanar distance measured from the adjacent lattice fringes is about 0.26 nm for the face centered cubic (FCC) structure of silver. The EDS analysis of SiO_2/Ag and Ag nanoparticles suggests that the SiO_2 nanoparticles contain only Si and oxygen elements (Fig. S2a†) where the Ag nanoparticles contain only the Ag element (Fig. S2b†). Fig. 8d shows the photographs of the three samples of SiO_2, SiO_2/Ag and Ag nanoparticles, which display clearly the white color of SiO_2, the yellow color of Ag and the brownish color of SiO_2/Ag.

Catalytic efficiency

Scheme 2 shows the general reduction reaction of 4-nitroaniline to 4-phenylenediamine in the presence of the produced Fe_3O_4/SiO_2/Ag nanocubes and $NaBH_4$. The produced 4-phenylenediamine as a reduction product of 4-nitroaniline is considered a useful and an attractive intermediate in the preparation of polymers, hair dyes, and rubber products.[50–52] The catalytic reduction reaction of 4-nitroaniline is easily monitored *via* UV-vis spectroscopy through the decrease in the strong adsorption of the 4-nitroanilinate anion at approximately 380 nm. The reference UV-vis spectrum of 4-phenylenediamine is shown in Fig. S3a.† Before investigating the catalytic efficiency of our synthesized nanocubes, we performed an experiment monitoring the reduction of 4-nitroaniline with $NaBH_4$ in the absence of nanoparticles. From the UV figure, a slow decrease in the characteristic absorbance of 4-nitroaniline at 380 nm even after aging the solution for 1 day occurred. Only approximately 3% of the compound was reduced (please see ESI Fig. S3b†), which indicated that a kinetic barrier prevents the electron transfer from the donor BH_4^- to the acceptor 4-nitroaniline. The catalytic ability of an equal amount of pristine iron oxide nanocubes was studied. As observed in Fig. 9a, a minimal effect was noted on the change in the absorbance band at 380 nm within 60 min of reaction time, emphasizing that the Fe_3O_4 nanocubes do not play a role in the catalytic efficiency for the reduction reaction of 4-nitroaniline.

However, a significantly decreased absorption intensity for the 4-nitroaniline at 380 nm occurred when Fe_3O_4/SiO_2/Ag nanocubes were used as a catalyst material (Fig. 9b). The dramatic decrease in the peak intensity at 380 nm was accompanied by the appearance of one peak at 240 nm, attributed to the formation of 4-phenylenediamine.[53] The reduction reaction occurred *via* relaying electrons from the donor BH_4^- to the acceptor 4-nitroaniline after the adsorption of both compounds onto the surface of the Fe_3O_4/SiO_2/Ag nanocubes. The hydrogen atom, formed from hydride after the electron transfer (ET) to the Ag nanodots, attacked and reduced 4-nitroaniline molecules.[1,54]

Notably, a complete reduction of 4-nitroaniline using our synthesized Fe_3O_4/SiO_2/Ag nanocubes occurred within 200 seconds of starting the reaction. Catalytic activities are

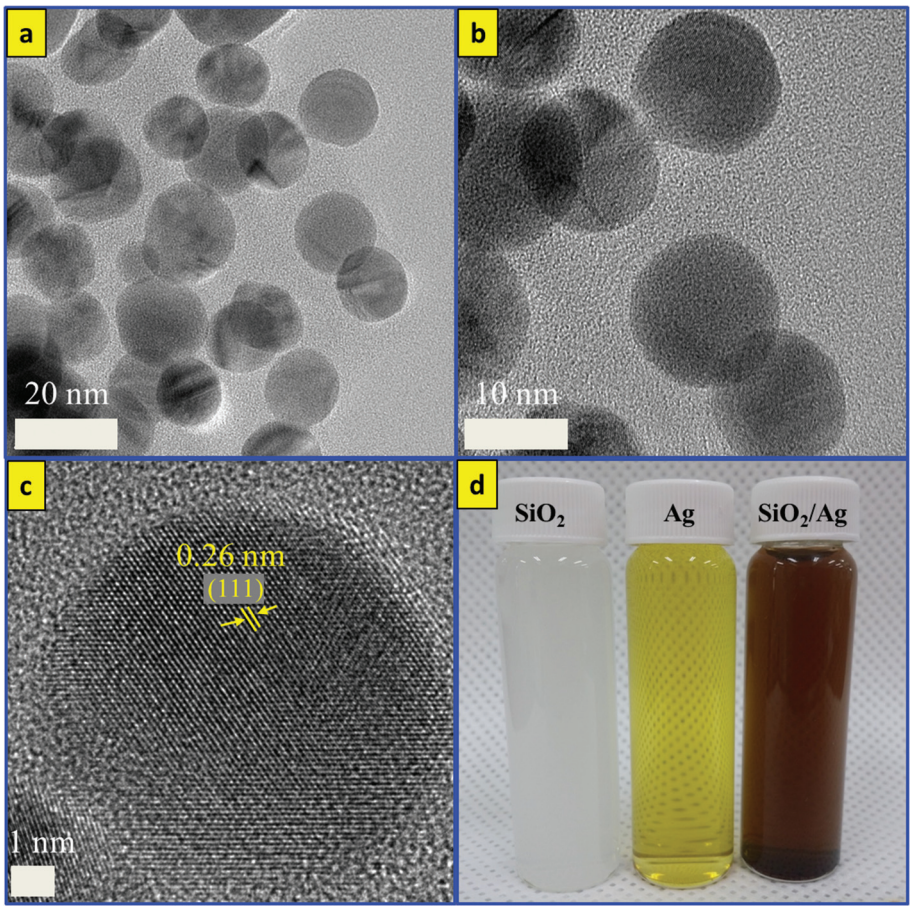

Fig. 8 TEM images of (a, b) Ag nanoparticles, (c) HRTEM of Ag NPs, and (d) photographic images of SiO_2, Ag and SiO_2/Ag NPs display their different colors.

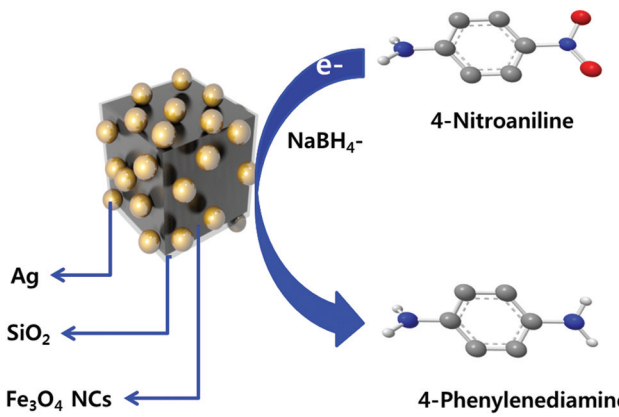

Scheme 2 Schematic diagram outlining the reduction reaction of 4-nitroaniline to 4-phenylenediamine using Fe_3O_4/SiO_2/Ag nanocubes.

mainly determined by two key parameters such as the availability of active surface area and the catalyst active sites on the surface for the electron transfer, removing the kinetic barrier.[55] The superior catalytic properties of our functionalized nanocubes were attributed to the high surface activity of the silver nanodots and the high surface area of the cubic shape of magnetite compared with various other shapes.[1,30,31] The self-assembled aggregated Ag nanodots are not fully uniform, displaying a higher number of corner and edge atoms. Additionally, the dendritic structure of Ag NPs displays a higher number of edges and corners, potentially increasing the catalytic reaction rates.[56] Even though a similar behavior of complete reduction of 4-nitroaniline to 4-phenylenediamine was observed when both Ag and SiO_2/Ag nanoparticles are used as a catalyst, the reduction times are 10 and 16 minutes, respectively, which is longer than that for Fe_3O_4/SiO_2/Ag nanoparticles. The catalytic activity of Ag nanoparticles is in good agreement with the previously reported Baruah *et al.* method, where they succeeded in completely reducing 4-nitrophenol to 4-aminophenol using stabilized Ag NPs within 10 minutes.[57] Fig. S4(a, b)† show the UV-vis absorption spectra for the reduction of 4-nitroaniline to 4-phenylenediamine in the presence of Ag as well as SiO_2/Ag nanoparticles. From the figure, and as expected, a decrease in the peak intensity at 380 nm was observed because of the catalytic activity of silver as we explained above. However, a little longer time is needed for the achievement of complete reduction of 4-nitroaniline than the

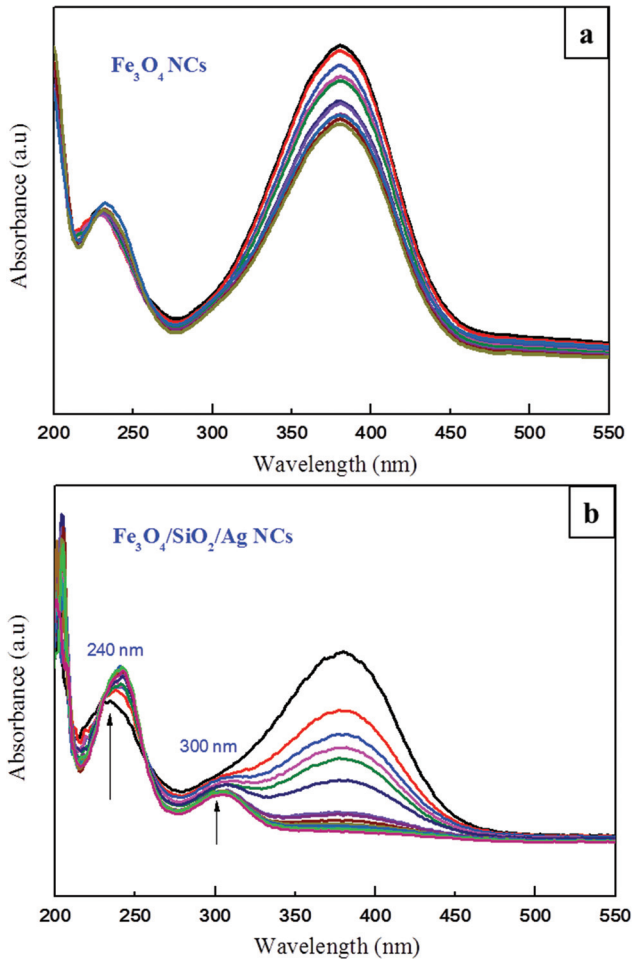

Fig. 9 UV-visible spectra for the reduction reaction of a 4-nitroaniline compound by (a) Fe_3O_4 nanocubes and (b) $Fe_3O_4/SiO_2/Ag$ nanocubes obtained at various times.

time taken in the case of $Fe_3O_4/SiO_2/Ag$ nanocubes. The reason for such a time difference may be attributed to the presence of Fe^{2+} in the Fe_3O_4 structure, which enhances the production rate of $^{\bullet}OH$.[25,29]

The most important advantages for the usage of the produced sample in this type of catalyst applications are mainly the ease of recycling by magnetic separation compared with using the silver nanoparticles. The reusability experiments of $Fe_3O_4/SiO_2/Ag$ nanocubes demonstrated that approximately 88% of 4-nitoaniline was reduced even after a fifteen-cycle run for the reduction process (Fig. 10). This result shows that this nanocube catalyst is highly stable because of the unique core/shell structure and therefore can be used for repeated 4-nitroaniline reduction reactions. Additionally, the catalytic activity of several recently reported highly active catalysts were compared with our synthesized material. For samples of spherical $Fe_3O_4/SiO_2/Ag$ nanoparticles, several groups have succeeded in reducing 4-nitrophenol (a nitro organic compound) within a reaction time between 10 and 14 min[1,31,58] with nearly identical

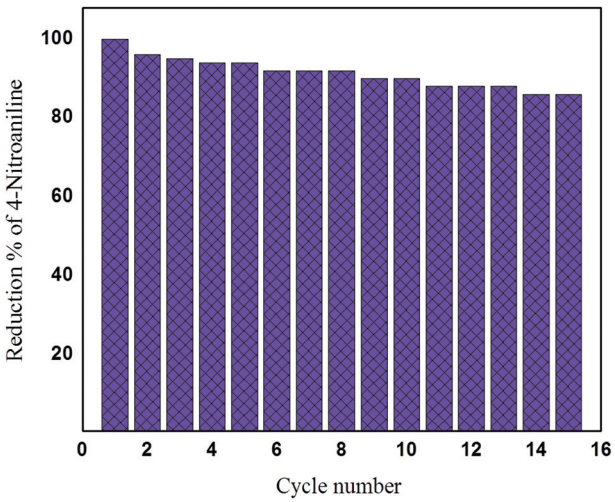

Fig. 10 The recycling curves of the catalyst sample ($Fe_3O_4/SiO_2/Ag$ nanocubes) for 15 repetitions.

concentration of materials. Nevertheless, other groups have succeeded in completely converting 4-nitrophenol to 4-aminophenol within 240–300 seconds; however, they substituted the silver with expensive gold nanoparticles within the identical structure of $MNPs/SiO_2/Au$ nanoparticles.[59–61] By contrast, in this study, we used a simple, reliable, economic, eco-friendly and highly efficient sonochemical approach to synthesize $Fe_3O_4/SiO_2/Ag$ nanocubes with an excellent catalytic efficacy in a short time.

Conclusion

In summary, we have demonstrated a novel sonochemical approach for the facile synthesis of $Fe_3O_4/SiO_2/Ag$ nanocubes, Ag NPs and SiO_2/Ag NPs. The produced $Fe_3O_4/SiO_2/Ag$ nanocubes displayed superior catalytic properties to Ag NPs and SiO_2/Ag NPs for 4-nitroaniline reductions with recycling properties up to 15 cycles and 88% efficiency. The novel multilayer core/shell nanocubes can be extended to other applications such as biomedical detection, energy conversion and storage systems. Further, the developed sonochemical approach in this study is expected to be a promising route for the synthesis of various types of core/shell nanostructures of $MNPs/SiO_2$/noble metals because this method is facile, reliable, economical and eco-friendly.

Acknowledgements

This work was supported by the Samsung Research Funding Center of Samsung Electronics under project number SRFC-MA1402-01.

References

1 X. Du, J. He, J. Zhu, L. Sun and S. An, *Appl. Surf. Sci.*, 2012, **258**, 2717–2723.
2 L. Liu, F. Ni, J. Zhang, X. Jiang, X. Lu, Z. Guo and R. Xu, *Acta Biochim. Biophys. Sin.*, 2011, **43**, 316.
3 W. Lesniak, A. U. Bielinska, K. Sun, K. W. Janczak, X. Shi, J. R. Baker and L. P. Balogh, *Nano Lett.*, 2005, **5**, 2123–2130.
4 J. E. Skebo, C. M. Grabinski, A. M. Schrand, J. J. Schlager and S. M. Hussain, *Int. J. Toxicol.*, 2007, **26**, 135–141.
5 S. Kumar, N. Harrison, R. K. Richards and K. Sokolov, *Nano Lett.*, 2007, **7**, 1338–1343.
6 A. M. Schrand, L. K. Braydich-Stolle, J. J. Schlager, L. Dai and S. M. Hussain, *Nanotechnology*, 2008, **19**, 1–13.
7 R. Xu, J. Ma, X. Sun, Z. Chen, X. Jiang, Z. Guo and L. Huang, *Cell Res.*, 2009, **19**, 1031–1034.
8 M. Mahmoudi and V. Serpooshan, *ACS Nano*, 2012, **6**, 2656–2664.
9 B. Chudasama, A. K. Vala, N. Andhariya, R. V. Upadhyay and R. V. Mehta, *Nano Res.*, 2009, **2**, 955–965.
10 L. Wang, J. Luo, S. Shan, E. Crew, J. Yin and C. J. Zhang, *Anal. Chem.*, 2011, **83**, 8688–8695.
11 M. S. Mauter, Y. Wang, K. C. Okemgbo, C. O. Osuji, E. P. Giannelis and M. Elimetech, *ACS Appl. Mater. Interfaces*, 2011, **3**, 2861–2868.
12 M. Liong, B. France, K. A. Bradley and J. I. Zink, *Adv. Mater.*, 2009, **21**, 1684–1689.
13 S. Tang, S. Vongehr and X. Meng, *J. Phys. Chem. C*, 2010, **114**, 977–982.
14 P. Zhang, C. Shao, Z. Zhang, M. Zhang, J. Mu, Z. Guo and Y. Liu, *Nanoscale*, 2011, **3**, 33573363.
15 H. L. Liua, P. Houa, W. X. Zhanga and J. Wu, *Colloids Surf., A*, 2010, **356**, 21–27.
16 S. Laurent, D. Forge, M. Port, A. Roch, C. Robic, L. V. Elst and R. N. Muller, *Chem. Rev.*, 2008, **108**, 2064.
17 H. Pardoe, W. Chua-anusorn, T. G. S. Pierre and J. Dobson, *J. Magn. Magn. Mater.*, 2001, **225**, 41.
18 L. Josephson, J. M. Perez and R. Weissleder, *Angew. Chem., Int. Ed.*, 2001, **40**, 3204.
19 A. K. Gupta and M. Gupta, *Biomaterials*, 2005, **26**, 3995.
20 H. L. Liu, S. P. Ko, J. H. Wu, M. H. Jung, J. H. Min, J. H. Lee, B. H. An and Y. K. Kim, *J. Magn. Magn. Mater.*, 2007, **310**, 815.
21 H. Y. Lee, S. H. Lee, C. Xu, J. Xie, J. H. Lee, B. Wu, A. L. Koh, X. Wang, R. Sinclair, S. X. Wang, D. G. Nishimura, S. Biswal, S. Sun, S. H. Cho and X. Chen, *Nanotechnology*, 2008, **19**, 165101.
22 S. R. Dave and X. Gao, *Wiley Interdiscip. Rev.: Nanomed. Nanobiotechnol.*, 2009, **1**, 583–609.
23 J. M. Jeong, B. G. Choi, S. C. Lee, K. G. Lee, S. J. Chang, Y. K. Han, Y. B. Lee, H. U. Lee, S. Kwon, G. Lee, C. S. Lee and Y. S. Huh, *Adv. Mater.*, 2013, **25**, 6250–6255.
24 S. R. Pouran, A. Abdul Raman and W. M. A. W. Daud, *J. Cleaner Prod.*, 2014, **64**, 24–35.
25 W. P. Kwan and B. M. Voelker, *Environ. Sci. Technol.*, 2003, **37**, 1150–1158.
26 B. W. Tyre, R. J. Watts and G. C. Miller, *J. Environ. Qual.*, 1991, **20**, 832–838.
27 S. H. Kong, R. J. Watts and J. H. Choi, *Chemosphere*, 1998, **37**, 1473–1482.
28 S. Yang, H. He, D. Wu, D. Chen, X. Liang, Z. Qin, M. Fan, J. Zhu and P. Yuan, *Appl. Catal., B*, 2009, **89**, 527–535.
29 M. Abbas, B. P. Rao, V. Reddy and C. Kim, *Ceram. Int.*, 2014, **40**, 11177–11186.
30 K. S. Shin, Y. K. Cho, J. Y. Choi and K. Kim, *Appl. Catal., A*, 2012, **413–414**, 170–175.
31 Y. Chi, Q. Yuan, Y. Li, J. Tu, L. Zhao, N. Li and X. Li, *J. Colloid Interface Sci.*, 2012, **383**, 96–102.
32 X. Wang, Y. Dai, J. l. Zou, L. Y. Meng, S. Ishikawa, S. Li, M. Abuobeidahd and H. g. Fu, *RSC Adv.*, 2013, **3**, 11751–11758.
33 A. Bayat, M. S. Fard, N. Ehyaei and M. M. Hashemi, *RSC Adv.*, 2015, **5**, 22503–22509.
34 M. Kooti, S. Gharineh, M. Mehrkhah, A. Shaker and H. Motamedi, *Chem. Eng. J.*, 2015, **259**, 34–42.
35 M. Abbas, M. Takahashi and C. Kim, *J. Nanopart. Res.*, 2013, **15**, 1354–1366.
36 M. Abbas, S. Torati, C. S. Lee, C. Rinaldi and C. Kim, *J. Nanomed. Nanotechnol.*, 2014, **5**, 6.
37 N. Ghows and M. H. Entezari, *Ultrason. Sonochem.*, 2012, **19**, 1070–1078.
38 D. Radziuk, D. Grigoriev, W. Zhang, D. Su, H. Mohwald and D. J. Shchukin, *Phys. Chem. C*, 2010, **114**, 1835–1843.
39 V. G. Pol, D. N. Srivastava, O. Palchik, V. Palchik, M. A. Slifkin, A. M. Weiss and A. Gedanken, *Langmuir*, 2002, **18**, 3352–3357.
40 C. Hui, C. Shen, J. Tian, L. Bao, H. Ding, C. Li, Y. Tian, X. Shi and H. J. Gao, *Nanoscale*, 2011, **3**, 701–705.
41 J. H. Bang and K. S. Suslick, Application of ultrasound to the synthesis of nanostructured materials, *Adv. Mater.*, 2010, **22**, 1039–1059.
42 F. Dang, N. Enomoto, J. Hojo and K. Enpuku, *Ultrason. Sonochem.*, 2009, **16**, 649–654.
43 K. S. Suslick and G. J. Price, *Annu. Rev. Mater. Sci.*, 1999, **29**, 295–326.
44 Y. K. Sun, M. Ma, Y. Zhang and N. Gu, *Colloids Surf., A*, 2004, **245**, 15–19.
45 B. D. Cullity and S. R. Stock, *Elements of X-Ray Diffraction*, Prentice-Hall, Englewood Cliffs, NJ, 3rd edn, 2001.
46 M. Abbas, B. P. Rao and C. Kim, *Mater. Chem. Phys.*, 2014, **147**, 443451.
47 X. Wang, L. Wang, X. He, Y. Zhang and L. Chen, *Talanta*, 2009, **78**, 327–332.
48 A. Henglein, *Chem. Mater.*, 1998, **10**, 444–450.
49 T. Sinha, M. Ahmaruzzaman and A. Bhattacharjee, *J. Environ. Chem. Eng.*, 2014, **2**, 2269–2279.
50 C. Franco, *Eur. Polym. J.*, 1996, **32**, 43–50.
51 L. H. Shu and L. Y. Wen, *Ann. Occup. Hyg.*, 2009, **53**, 289–296.
52 I. Yoshiaki and K. Masaaki, *J. Health Sci.*, 2000, **46**, 467–473.
53 M. Kumar and S. Deka, *ACS Appl. Mater. Interfaces*, 2014, **6**, 16071–16081.

54 B. Naik, S. Hazra, V. S. Prasad and N. N. Ghosh, *Catal. Commun.*, 2011, **12**, 1104–1108.
55 S. Kundu and M. Jayachandran, *RSC Adv.*, 2013, **3**, 16486–16498.
56 D. Huang, X. Bai and L. Zheng, *J. Phys. Chem. C*, 2011, **115**, 14641.
57 B. Baruah, G. J. Gabriel, M. J. Akbashev and M. E. Booher, *Langmuir*, 2013, **29**, 4225–4234.
58 H. Woo, K. Lee, S. Park and K. H. Park, *Molecules*, 2014, **19**, 699–712.
59 F. H. Lin and R. A. Doong, *Appl. Catal., A*, 2014, **486**, 32–41.
60 J. Zheng, Y. Dong, W. Wang, Y. Ma, J. Hu, X. Chen and X. Chen, *Nanoscale*, 2013, **5**, 4894–4901.
61 S. Zhang, S. Gai, F. He, Y. Dai, P. Gao, L. Li, Y. Chen and P. Yang, *Nanoscale*, 2014, **6**, 7025–7032.